A Computational Procedure for Instationary Temperature Dependent Snow Creep

Perry Bartelt[1] and Marc Christen[2]

[1] Head Avalanche Dynamics and Numerics, Swiss Federal Institute for Snow and
    Avalanche Research, CH 7260 Davos Dorf, Switzerland, bartelt@slf.ch
[2] Engineer,Swiss Federal Institute for Snow and Avalanche Research, CH 7260
    Davos Dorf, Switzerland, christen@slf.ch

Abstract. A computational procedure to model instationary creep movements in alpine snowpacks is presented. The model allows the study of large volumetric and shear strains (new snowfall), temperature dependent material behaviour (sudden warming) and progressive creep fracture. These processes are all important factors in natural avalanche release. A viscoelastic material model for snow is proposed in which the constitutive properties are characterized on planes of various orientations within the material. This model is conceptually simple because it does not employ complicated tensorial arguments. It is, however, capable of modelling the highly nonlinear and complex material behaviour of snow including the influence of material microstructure. The model requires only a few parameters which can be determined from simple uniaxial or triaxial experiments. The new constitutive model and numerical procedure is verified using two field and laboratory experiments.

1   Introduction

The purpose of this paper is to present a finite element based computational procedure to calculate instationary viscoelastic creep movements in alpine snowpacks. The procedure can model: (1) large volumetric and shear strains (0.50 to 1.00) and strain-rates (up to $10^{-3}\mathrm{s}^{-1}$) to allow the study of snowpack movements after a heavy snowfall and the settlement of new snow, (2) temperature dependent material behaviour (including phase change) to allow the study of sudden variations in meteorological conditions, such as a quick rise in temperature with strong winds (Föhn), (3) fracture or progressive creep damage of weak snow layers based on the crystal morphology of those layers and (4) the creep forces exerted on avalanche retaining structures.

We would like to emphasize that these modelling requirements are posed by avalanche warning specialists at our institute who are now beginning to use physical snowpack models on a day-to-day operational basis [1], [2]. The determination of the maximum creep force exerted on defense structures is also an important engineering task for the safety of many mountain communities.

The finite element method has been employed to simulate snowpacks [3], [4], [5], [6]; however, these calculations have all made the assumption of

stationary strain-rates and small deformations and strains. They are not adequate to postulate and quantify theories of avalanche formation, especially immediately after a new snowfall when the snowpack creep velocities are clearly instationary. In the snow settlement experiments of de Quervain, 1945, [7], which are modelled in this paper, snow increased in density from 120 [kgm^{-3}] to over 300 [kgm^{-3}] from self-weight alone in a period of 100 days. The experiments clearly showed that the settlement velocities reached a constant deformation velocity only after 70 days. Moreover, instationary creep behaviour dominated the duration of the experiments.

The greatest difficulty in the modelling of these processes is to formulate a constitutive law for snow that is both simple, i.e. it can be well understood intuitively, while, at the same time, it is elaborate enough to treat highly nonlinear and complex material behaviour. These goals are clearly at odds with each other. A further requirement is that the constitutive theory be expanded to consider the influence of snow micro-structure on material response. Of particular importance is the modelling of the strength of the snow-crystal bonds or necks. Of course, the law must also be directly verifiable by both field and laboratory experiments.

In the first part of this paper the constitutive model and the large-strain, rate-dependent plane strain finite element numerics are presented. The constitutive model does not employ over-complicated theories to describe viscoelastic snow behaviour [8], [9] or fracture [10]. These theories are both conceptually difficult and require complex experiments (shear tests) to determine the material parameters. Furthermore, they neglect the influence of snow microstructure.

In our approach the constitutive properties are characterized using simple one-dimensional material laws on planes with various orientations within the material. The overall material response, including shear resistance, is found by superimposing the response of the individual directions. This facilitates a better understanding of the material behaviour and, most importantly, the constitutive law requires fewer parameters which can be determined using simple temperature dependent uniaxial or triaxial tests. (Traxial creep tests using a specially designed triaxial apparatus for snow are presently being performed at our institute.) Finally, since the material laws are one-dimensional it is much easier to introduce microstructural parameters (grain size and shape, bond strength, neck length) into the constitutive model. Above all, fracture criteria based on snow microstructure can be easily formulated. The proposed model is based on so-called "microplane" models that have been successfully used to simulate progressive tensile fracturing and/or damage of aggregate materials such as concrete and rock [11], [12], [13].

The model is verified using both field and laboratory experiments. The 100-day creep experiments of de Quervain [7] and the snow settlement experiments of Kojima [14] are simulated with a high degree of accuracy.

2   Microplane Material Laws for Snow

Snow is a porous material consisting of ice grains and air. The ice grains have different shape and size depending on the thermodynamical and mechanical history of the snow. The ice grains are bonded together at so-called necks to form complex load carrying chains. The response of snow under loading is primarily a function of (1) the number of chains, which is usually described by the snow density, (2) the strength of the individual grain bonds, (3) the grain size and (4) the neck length. The deformation rate plays an important role on overall material behaviour since the ability of snow to form new load carrying chains and the strength of the ice bonds is rate dependent. In summary, the mechanical behaviour of snow is strongly dependent on the microstructural parameters of the ice matrix and the rate of applied loading. The constitutive modelling, however, is made even more difficult by the fact that the microstructure parameters are persistently changing under an applied temperature gradient and overburden pressure. Fig. 1 shows an idealized schematic representation of snow consisting of ice grains, grain bonds and load chains.
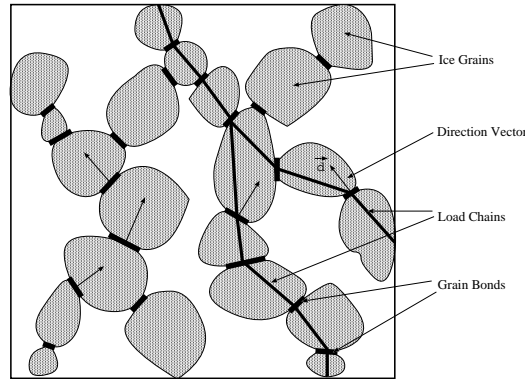
Fig. 1. Snow microstructure with microplane directions

In our model for snow creep and fracture, the constitutive laws are defined on planes of various orientations within the material. Bazant [11] called these planes "microplanes" because the inelastic material behaviour of each plane is based on the mechanics of the material microstructure. He introduced the prefix "micro" in order to emphasize the fact that for many materials the mechanical behaviour, especially fracture and damage, is best characterized on weak planes that are found in the material microstructure, specifically the interaggregate contact planes which, for the case of snow, are the ice grain bonds and necks.
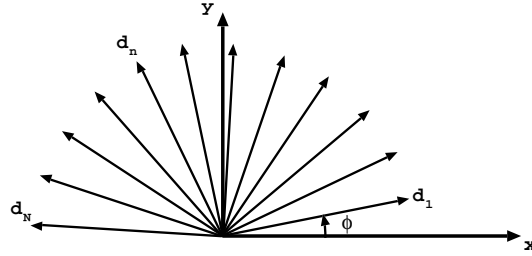
The behaviour of the individual microplanes is described by simple one-dimensional rheological material laws relating the normal stresses and strains in a single direction. We postulate that the mechanical behaviour and strength of the ice grain chains is more realistically and more simply described by the N-directional one-dimensional laws than complicated tensorial constitutive laws with many parameters. In a first approximation shear strains in the microplane directions are unopposed. However, this does not imply that the material as a whole has no shear stiffness: shear deformations are resisted by the normal stiffness of each microplane. The total material response is found by superimposing the contributions from all directions.

The strain on any microplane n is the resolved component of the macroscopic strain E_{ij} defined with respect to a Cartesian coordinate system. For plain strain:

$$\epsilon_n = d_{in} d_{jn} E_{ij} \qquad \text{for} \qquad i,j = 1,2 \qquad (\text{No sum on n}), \tag{1}$$

where d_{1n} and d_{2n} are the components of the n-th unit direction vector d_n, see Fig. 2, and are defined according to

$$d_n = \left\{ \begin{array}{c} d_{1n} \\ d_{2n} \end{array} \right\} = \left\{ \begin{array}{c} \cos(\phi - \frac{(n-1)\pi}{N}) \\ \sin(\phi - \frac{(n-1)\pi}{N}) \end{array} \right\}. \tag{2}$$

Fig. 2. The direction vectors d_n for $n = 1$ to N. As a first approximation, we assume that snow is an isotropic material and that the direction vectors are equally distributed.

We term ϵ_n the microstructure strain or the N-directional strain. In matrix form (1) can be written as

$$\{\epsilon\} = [D]\{E\}. \tag{3}$$

Relation (1) is termed a kinematic constraint since the strain in the $n-th$ direction is related to the macroscopic state of deformation. According to

Bazant [11], this approach physically models the behaviour of brittle aggregate materials better than by assuming that the microstresses in the N-directions correspond to the macroscopic stress. The stresses in a porous granular material like snow are far from uniform having very high stress concentrations at the snow crystal bonds: the microscopic stress state varies significantly from the macroscopic stress field. The kinematic constraint (1), however, ensures that the relative displacements between the ice crystals are approxiamated by the macroscopic strain field. This is a much better assumption, especially when formulating constitutive laws with fracture.

A further constraint is introduced into the microplane constitutive formulation. Namely that the N-directional stress components σ_n and Cartesian components S_{ij} which are work conjugate to the strains, ϵ_n and E_{ij}, respectively, must fulfill the scalar work equation,

$$S_{ij}E_{ij} = \sum_{n=1}^{N} \sigma_n \epsilon_n = \sum_{n=1}^{N} \sigma_n d_{in} d_{jn} E_{ij}. \tag{4}$$

The macroscopic Cartesian stress is thus related to the N-directional stress according to

$$S_{ij} = \sum_{n=1}^{N} d_{in} d_{jn} \sigma_n. \tag{5}$$

The above equation implies that the macroscopic state of stress, S_{ij} is found by superimposing the N-directional stresses. The stress σ_n represents the one-dimensional stress in the $n - th$ direction.

The vector d_n is defined in the undeformed coordinate system x_i. The angle ϕ is an arbitrary angle, usually set to $\phi = 0°$.

3   Viscoelastic N-Directional Material Models

In this section we formulate several one-dimensional, scalar material laws relating σ_n to ϵ_n (and not the tensors S_{ij} and E_{ij}). The N-directional constitutive formulation must meet a simple requirement: small strain linear isotropic elasticity will be modelled exactly. In this case the stress S_{ij} is related to the elastic strain E_{ij} according to the well known relation

$$S_{ij} = 2\mu E_{ij} + \lambda \gamma \tag{6}$$

where μ and λ are the Lamé constants and γ is the volumetric strain. The corresponding N-directional material law is

$$\sigma_n = \alpha \epsilon_n^e + \beta \gamma^e; \tag{7}$$

where α and β are material constants with the values

$$\alpha = \frac{8\mu}{N} = \frac{4C}{N(1+\nu)} \tag{8}$$

and

$$\beta = \frac{2\lambda - \mu}{N} = \frac{C}{N}\frac{4\nu - 1}{(1+\nu)(1-2\nu)} \tag{9}$$

The superscript e has been introduced to denote that the quantities ϵ_n and γ refer to the elastic N-directional and volumetric strains. The symbol C denotes the modulus of elasticity and ν Poisson's ratio. Note that when $\nu = 0.25$ then $\beta = 0$ and $\alpha = \frac{16}{5}\frac{C}{N}$. According to Mellor [15], $\nu = 0.25$ for medium to high density snow ($300 \leq \rho \leq 500$). For smaller densities ($\rho \leq 300$), $\nu \approx 0.20$.
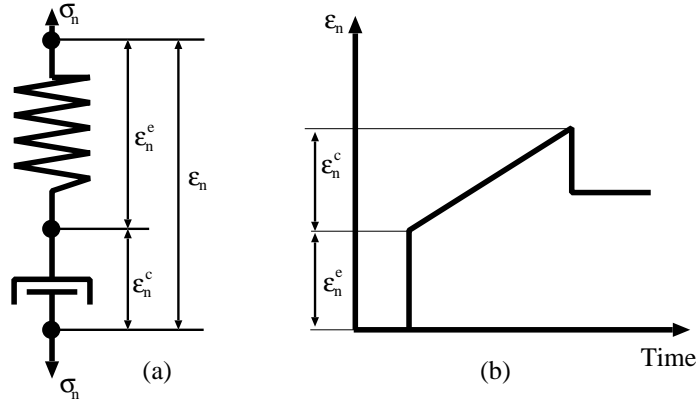
Fig. 3. (a) A visco-elastic Maxwell model describes the stress-strain relation in the $n - th$ direction. (b) Strain response of a Maxwell model under constant load.

Viscous behaviour (creep) is introduced into the N-directional material model by assuming that the total strain in the n-th direction is composed of elastic and viscous parts, i.e.,

$$\epsilon_n = \epsilon_n^e + \epsilon_n^c. \tag{10}$$

Also, the total volumetric strain is likewise decomposed into elastic and viscous parts of:

$$\gamma = \gamma^e + \gamma^c. \tag{11}$$

Thus, the N-directional material law (7) is rewritten as

$$\sigma_n = \alpha(\epsilon_n - \epsilon_n^c) + \beta(\gamma - \gamma^c). \tag{12}$$

Moreover, a simple Maxwell model is used to describe viscoelastic material behaviour. Of course, more complicated models are possible. Our motivation behind using this simple model in a first approximation is to demonstrate that even long time creep experiments and field tests can be modelled adequately with this law. The Maxwell model defines the viscous strain rate according to

$$\dot{\epsilon}_n^c = \frac{\sigma_n}{\eta} \tag{13}$$

The parameter η is termed the snow viscosity (with dimensions Pa s). Usually, the viscosity is defined as a function of the snow density and temperature $\eta = f(\rho, T)$. Several of the different laws are listed in the Table 1.

Table 1. Different constitutive laws for the compactive viscosity η.

Author (Year)	Viscosity [Pa s]
Kojima (1974) [14]	$\eta = 8.64(10^6)e^{0.021\rho}$
Mellor (1975) [15]	$\eta = 5.0(10^7)e^{0.022\rho}$
Claus (1978) [16]	$\eta = 6.57(10^7)e^{0.014\rho}$
Gubler (1994) [17]	$\eta = 1.86(10^{-6})e^{0.02\rho + 8100/T}$
Morris (1994) [18]	$\eta = 5.38(10^{-3})e^{0.024\rho + \frac{6042}{T}}$
Loth (1993) [19]	$\eta = 3.70(10^7)e^{8.10(10^{-2})(273.15-T)}e^{2.10(10^{-2})\rho}$

4 N-dimensional Constant Strain Triangular Elements

In this section the principle of virtual work (see, for example, Crisfield [20]),

$$W = W_i - W_e = \int_V \{S\}^T \{\delta E\} \, dV - W_e \tag{14}$$

is invoked in order to derive the tangent stiffness matrix and internal force vector of the N-directional plane strain triangular elements. In the equation above, W is the virtural work, W_i is the internal virtual work and W_e is the external virtual work. The internal virtual work is presently expressed in terms of the energy conjugate virtual Green's strains, δE, and the second Piola-Kirchhoff stress, S, which are both defined in a Cartesian coordinate system.

In the following the virtual work expression will be rewritten using the N-directional stress and strain measures presented in the previous section. As

stated in the introduction, our goal is to develop a continuum finite element that employs simple one-dimensional visco-elastic constitutive relations. This implies finding the N-directional virtual strains.

Viscous creep deformations are produced by introducing creep forces on the right-hand side of the equilibrium equations. These "pseudo-loads" enforce the viscous strain rates predicted by the viscous creep law. Thus, another important task of this section is to derive the creep "pseudo-load" vector.

In the next section, the computational procedure used to solve the global finite element equations, which is found by assembling the element stiffness matrices and force vectors, will be discussed.

Unlike the usual finite element formulation where the strains are found from the element-deformation gradient in the Cartesian directions, in this formulation the strains are calculated from the element side deformations. This is computationally efficient; however, it does introduce notational difficulties since a third strain measure arises. In the following a small e is used to denote the finite element side strains. Since the strains in the N-directions ϵ are finally used in the constitutive formulation, it does not matter whether the Cartesian strains E or element-side strains e are resolved into the N-directions.

As in the previous section, the superscripts e and v will be used to distinguish between the elastic and viscous strains in the N-directions, ϵ^e and ϵ^v, respectively. Also, the subscripts s and n are used to denote an element side and the n-th direction. The superscript t will be used to define the element configuration at time t and the superscript 0 will be used to denote the undeformed element configuration, $t = 0$.

Consider Fig. 4 which depicts a finite element triangle with area A.

For the deformed state at time $t > 0$ the Green-Lagrange strain of element side s is:

$$e_s = \frac{{}^tL_s^2 - {}^0L_s^2}{2({}^0L_s^2)} = \frac{\Delta x_s^2 + \Delta y_s^2 - {}^0L_s^2}{2({}^0L_s^2)} \qquad \text{for} \qquad s = 1, 2, 3. \qquad (15)$$

where ${}^0L_s^2$ and ${}^tL_s^2$ are the lengths of side s at the beginning of the analysis and time t, respectively. Note that for a pure rigid-body rotation the side strains are $e_s = 0$ for $s = 1, 2, 3$. The values Δx_s and Δy_s are found according to

$$\Delta x_s = {}^tx_i - {}^tx_j \text{ and } \Delta y_s = {}^ty_j - {}^ty_i \text{ for } i = 3, 1, 2 \text{ and } j = 2, 3, 1. \quad (16)$$

The Green-Lagrange side strains are found with respect to the undeformed side lengths ${}^0L_s^2$. The element side strains e_s are related to the Cartesian
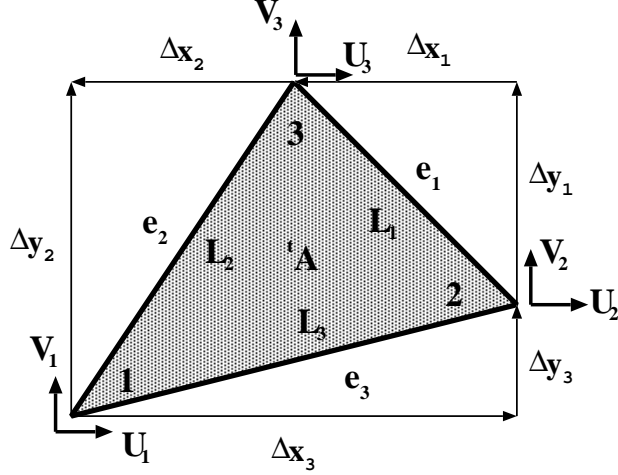
Fig. 4. Constant strain triangle.

Green-Lagrange strains E_{ij} by

$$\{e\} = \begin{Bmatrix} e_1 \\ e_2 \\ e_3 \end{Bmatrix} = \begin{bmatrix} \frac{\Delta x_1^2}{L_1^2} & \frac{\Delta y_1^2}{L_1^2} & \frac{2\Delta x_1 \Delta y_1}{L_1^2} \\ \frac{\Delta x_2^2}{L_2^2} & \frac{\Delta y_2^2}{L_2^2} & \frac{2\Delta x_2 \Delta y_2}{L_2^2} \\ \frac{\Delta y_3^2}{L_3^2} & \frac{\Delta y_3^2}{L_3^2} & \frac{2\Delta x_3 \Delta y_3}{L_3^2} \end{bmatrix} \begin{Bmatrix} E_{11} \\ E_{22} \\ E_{12} \end{Bmatrix} = [F] \{E\} \qquad (17)$$

From (3) the relationship between the side strains and N-directional strains can then be established

$$\{\epsilon\} = [D] \{E\} = [D][F]^{-1} \{e\} = [T_{ns}] \{e\}. \qquad (18)$$

The N x 3 matrix $[T_{ns}]$ resolves the side strains into the N-directions. Note that the elements of this matrix are only functions of the element shape at time $t = 0$, the undeformed configuration. It must be determined only once at the beginning of each calculation.

If a set of virtual nodal displacements,

$$\{\delta a\}^T = \{\delta U_1, \delta V_1, \delta U_2, \delta V_2, \delta U_3, \delta V_3\} \qquad (19)$$

is applied to the finite element, the virtual side strains are

$$\delta e_s = \frac{\Delta x_s}{^0L_s^2}\delta \Delta x_s + \frac{\Delta y_s}{^0L_s^2}\delta \Delta y_s = x_s(\delta U_i - \delta U_j) + y_s(\delta V_j - \delta V_i). \qquad (20)$$

where x_s and y_s are defined by setting

$$x_s = \frac{\Delta x_s}{^0L_s^2} \qquad \text{and} \qquad y_s = \frac{\Delta y_s}{^0L_s^2} \qquad (21)$$

Thus, the virtual strains can be expressed in matrix form as

$$\{\delta e\} = \left\{ \begin{array}{c} \delta e_1 \\ \delta e_2 \\ \delta e_3 \end{array} \right\} = \begin{bmatrix} 0 & 0 & -x_1 & -y_1 & x_1 & -y_1 \\ x_2 & -y_2 & 0 & 0 & -x_2 & y_2 \\ x_3 & y_3 & x_3 & -y_3 & 0 & 0 \end{bmatrix} \left\{ \begin{array}{c} \delta U_1 \\ \delta V_1 \\ \delta U_2 \\ \delta V_2 \\ \delta U_3 \\ \delta V_3 \end{array} \right\} = \left[{}^t\bar{B} \right] \{\delta a\} . \quad (22)$$

The superscript t is placed on the $[\bar{B}]$ matrix to emphasize that it is a function of the deformed element configuration. The virtual N-directional strains are subsequently related to the virtual finite element displacements according to

$$\{\delta\epsilon\} = [T_{ns}] \{\delta e\} = [T_{ns}] \left[{}^t\bar{B} \right] \{\delta a\} = \left[{}^tB \right] \{\delta a\} . \quad (23)$$

Rewriting the internal virtual work by using the N-directional stress and strain measures and then substituting the above epression relating the virtual element displacments to the virtual strains allows the definition of the finite element internal nodal forces $\{{}^tp_i\}$ at time t:

$$W_i = \int_A \{S\}^T \{\delta E\} \, dA = \int_A \{\sigma\}^T \{\delta\epsilon\} \, dA$$
$$= \{\delta a\}^T \int_A \left[{}^tB \right]^T \{{}^t\sigma\} \, dA = \{\delta a\}^T \{{}^tp_i\} . \quad (24)$$

Moreover,

$$\{{}^tp_i\} = \left[{}^tB \right]^T \{{}^t\sigma\} \, {}^tA. \quad (25)$$

The tangent-element-stiffness matrix $[K_T]$ is found by differentiating the internal forces (see Crisfield [20]), i.e.

$$d\{{}^tp_i\} = \left(d\left[{}^tB \right]^T \{{}^t\sigma\} + \left[{}^tB \right]^T d\{{}^t\sigma\} \right) {}^tA = [K_T] \, d\{a\} . \quad (26)$$

In the numerical calculations we neglect the geometric stiffness contribution, that is,

$$d\left[{}^tB \right]^T \{{}^t\sigma\} \approx 0. \quad (27)$$

The increment in stress is found from the N-directional stress strain relationship (7),

$$d\{\sigma\} = d\left(\alpha\epsilon^e + \beta\gamma^e \right) = \left(\frac{d\alpha}{d\epsilon^e} \epsilon^e + \alpha + \frac{d\beta}{d\epsilon^e} \gamma^e \right) d\epsilon^e + \beta \sum_{n=1}^{N} \frac{d\gamma^e}{d\epsilon_n^e} d\epsilon_n^e. \quad (28)$$

Assuming that the last term of the above equation is small,

$$\beta \sum_{n=1}^{N} \frac{d\gamma^e}{d\epsilon_n^e} d\epsilon_n^e \approx 0, \quad (29)$$

the diagonal elements C_n of an NxN material matrix $[C_T]$ can be defined by

$$C_n = \left(\frac{d\alpha}{d\epsilon_n^e}\epsilon_n^e + \alpha + \frac{d\beta}{d\epsilon_n^e}\gamma^e \right). \qquad (30)$$

The N-directional incremental stress-strain relationship is then

$$d\left\{{}^t\sigma\right\} = \left[{}^tC_T\right]d\epsilon^e = \left[{}^tC_T\right]\left[{}^tB\right]d\left\{a\right\}. \qquad (31)$$

This equation can be substituted into (26) to find

$$d\left\{{}^tp_i\right\} = \left[\left[{}^tB\right]^T\left[{}^tC_T\right]\left[{}^tB\right]{}^tA\right]d\left\{a\right\}. \qquad (32)$$

The element stiffness matrix is then by definition

$$[K_T] = \left[{}^tB\right]^T\left[{}^tC_T\right]\left[{}^tB\right]{}^tA. \qquad (33)$$

The approximations (27) and (29) are not significant for the accuracy of the numerical calculations since the stiffness matrix is used only to approximate the internal stress state. As will be shown in the next section, the equilibrium between the internal and external forces is always strictly enforced. However, the approximations could influence the number of computational iterations required to find equilibrium. In the numerical calculations a Poisson's ratio for snow of $\nu = 0.25$ is assumed, thus, $\beta = 0$ and (29) is exactly zero.

The increment in load produced by a creep deformation is

$$d\left\{{}^tp_c\right\} = \left[{}^tB\right]^T\left[{}^tC_T\right]d\left\{\epsilon^v\right\}{}^tA. \qquad (34)$$

These forces are applied to the finite element mesh in order to produce creep deformations corresponding to the time dependent viscous strain rates. In the calculation procedure we use an explicit scheme to find d $\left\{\epsilon^v\right\}$:

$$d\left\{\epsilon^v\right\} = \left\{\dot{\epsilon}^v\right\}\Delta t, \qquad (35)$$

where Δt is the time step increment of the time integration scheme.

Finally, a self-weight load, $\left\{{}^tp_e\right\}$, always acts on the system. This element force vector is calculated according to

$$\left\{{}^tp_e\right\}^T = \left\{0, -\frac{\rho g A}{3}, 0, -\frac{\rho g A}{3}, 0, -\frac{\rho g A}{3}\right\}, \qquad (36)$$

where g is the gravitational acceleration and ρ the density of the finite element. This vector is constant since the mass of each element remains unchanged during the calculation.

5   Solution of the Equilibrium Equations

The equations of equilibrium which must be satisfied at any instant of time t are the balance between internal and external nodal forces,

$$\left\{{}^t p_i\right\} + \left\{{}^t p_e\right\} = \int_A \left[{}^t B\right]^T \left\{{}^t \sigma\right\} dA + \left\{{}^t p_e\right\} = 0. \tag{37}$$

These equations can also be posited in incremental form

$$d\left\{{}^t p_i\right\} + d\left\{{}^t p_e\right\} = \int_A \left[{}^t B\right]^T d\left\{{}^t \sigma\right\} dA + d\left\{{}^t p_e\right\} = 0, \tag{38}$$

in which $d\left\{{}^t p_e\right\}$ is the change in external load during the time interval Δt. For our case, $d\left\{{}^t p_e\right\}$ is usually zero, except in the beginning of the analysis or during a new snowfall.

The displacement increment $d\{a\}$ which is calculated for the time step Δt is found according to

$$d\{a\} = \left[{}^t K_T\right]^{-1} d\{R\}, \tag{39}$$

where $d\{R\}$ is called the incremental pseudo-load vector containing the influence of the instationary creep effects of

$$d\{R\} = d\left\{{}^t p_c\right\} + d\left\{{}^t p_e\right\} = \int_A \left[{}^t B\right]^T \left[{}^t C_T\right] \left\{{}^t \dot{\epsilon}^v\right\} \Delta t dA + d\left\{{}^t p_e\right\}. \tag{40}$$

These calculations require the formation of the $\left[{}^t B\right]^T$ matrix for every element at every time step. This is not computationally demanding since the calclation of $\left[{}^t \bar{B}\right]$ needs only a few floating point operations, (22). It is then multiplied with the Nx3 matrix $[T_{ns}]$, see (23). This transformation matrix is formed only once at the beginning of a computation.

Because the calculation (40) is based on the linearized form of the equilibrium equations, (39), they will not satsify the equilibrium condition (38) exactly. Thus, several iterations may be required to satisfy (40) within some specified convergence criterion. The out-of-balance forces at the end of the time step are always added to the applied force increment $d\left\{{}^t p_e\right\}$ at the next time step.

In summary, the computational procedure is as follows:

1. At time t, the displacements $\left\{{}^t a\right\}$, N-directional stress $\left\{{}^t \sigma\right\}$ and external forces $\left\{{}^t p_e\right\}$ are known. To begin at $t = 0$, we set $\left\{{}^0 a\right\} = 0$. The initial stress state $\left\{{}^0 \sigma\right\}$ is determined from a small strain elastic analysis. The external load is self-weight.
2. The creep-strain rate in N-strain-directions is determined for every element,

$$\left\{{}^t \dot{\epsilon}^v\right\} = f\left({}^t \sigma_n, {}^t T, {}^t \rho\right), \tag{41}$$

according to a vicous law listed in Table 1. The creep strain increment in the nth-direction is thus

$$d\left\{\epsilon^v\right\} = \left\{{}^t\dot{\epsilon}^v\right\} \Delta t. \tag{42}$$

3. Find the NxN diagonal elasticity matrix $[C_T]$ from (30).
4. Construct the incremenatal creep force vector $d\{p_c\}$ according to (34) and add it to the incremental external load vector $d\{p_e\}$ to obtain the pseudo-load vector $d\{R\}$.
5. Construct the tangent stiffness matrix $[{}^tK_T]$ according to (33).
6. Calculate the increment in displacements $d\{a\}$ according to (39).
7. Calculate the increment in total strain and stress in N-directions for each element

$$d\{\epsilon\} = \left[{}^tB\right] d\{a\}. \tag{43}$$

$$d\{\sigma\} = [C_T]\left(d\{\epsilon\} - \{\dot{\epsilon}^v\}\Delta t\right). \tag{44}$$

8. Update the stress

$$\left\{{}^{t+\Delta t}\sigma\right\} = \left\{{}^t\sigma\right\} + d\{\sigma_n\}. \tag{45}$$

9. Update the displacements

$$\left\{{}^{t+\Delta t}a\right\} = \left\{{}^ta\right\} + d\{a\}. \tag{46}$$

Finally, note that the determination of the increment in creep strains $d\{\epsilon^v\}$ is based on an Euler time integration; that is, it is determined by the conditions existing at time t. This procedure is not unconditionally stable. Therefore, both the stability and the numerical results depend on the time step size Δt.

6   One-Hundred Day Laboratory Settlement Experiments of M. de Quervain, 1945

In order to determine long-term, temperature dependent snow settlement curves, De Quervain (1945) [7] filled eight wooden boxes (20cm x 20cm x 100cm) with 90 cm of sieved snow (grain size of 0.3mm) and measured the snow displacement and density distribution daily, see Fig. 5a and Fig. 5b. The experiment lasted 100 days, the first 40 days being investigated in this example. The experimental results are extremely well documented and are ideal first examples to test the computational procedure described in the first part of this paper.

De Quervain used the experiments to develop empirical settlement curves for inhomogeneous (multi-layer) snowpacks. At the time this was an improvement over the existing theory of Haefeli (1942) [21], which considered only
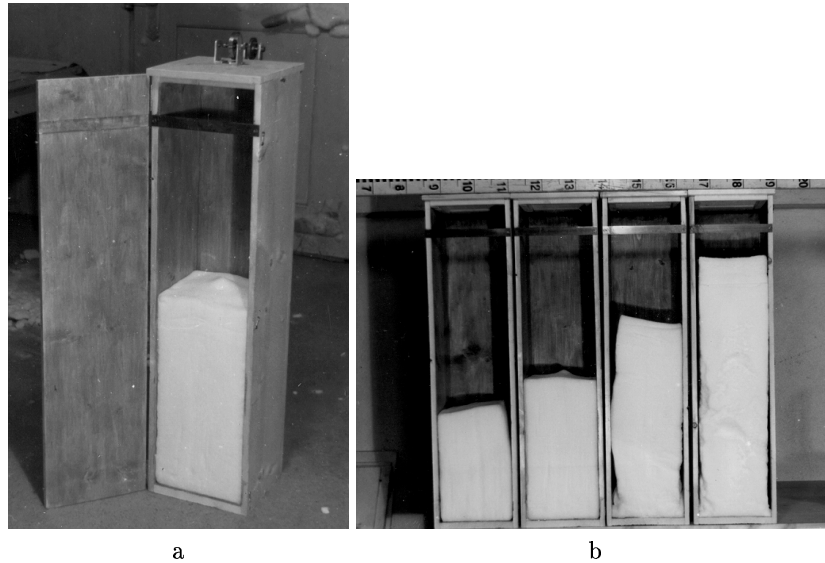
Fig. 5. a) Open wooden box showing the settlement measuring instrument on top of it; b) Wooden boxes after the 100 days settlement period, temperature boundary being -2C, -10C, -18.5C and -32.5C (from left to right).

homogeneous snow (single layer snowpacks) and was based on a purely empirical formula.

Although De Quervain realized that snow metamorphism and sublimation produced a settlement and mass loss, he was primarily interested in the time dependent mechanical deformation caused by self-weight and wind loads. He believed that the deformation of new snow was primarily caused by overburden stress, and not ice crystal changes, which occur at a much slower rate. For this reason De Quervain performed the experiments in the laboratory with homogeneous snow under constant temperature. The initial snow density was approximately 115 $[\text{kgm}^{-3}]$; the snow settled up to 50 cm and compacted to densities over 300 $[\text{kgm}^{-3}]$, depending on the test temperature. Four different temperatures were used: -2 C, -10 C, -18.5 C and -32.5 C. Ski-wax was used to mimimize the side wall friction of the wooden boxes.

Calculations were carried out, using different viscosity laws (see Table 1), and comparing them to the measured values. A 'best-fit' viscosity law (*Christen* viscosity law) was developed,

$$\eta = 2.0(10^{-8})\rho^{7.9} \qquad [\text{Pa s}] \qquad (47)$$

yielding very good results in this special experiment (see Table 3), but failing when used with other problems. Table 3 compares the measured and simulated settlement and density results.

Table 2. Initial simulation data.

Simulation Begin/End [days]	0 - 40
Initial Mesh Height [cm]	90
Initial Density [kgm^{-3}]	115
Initial Temperature [C]	-10

Table 3. Simulation results.

Simulation time	5 Days		40 Days	
Viscosity	Settlement	Density	Settlement	Density
	[cm]	[kgm^{-3}]	[cm]	[kgm^{-3}]
	Δh	Top/Base	Δh	Top/Base
Measurements	20.0	150/188	39.8	186/288
Kojima	54.8	125/496	-	-
Mellor	25.7	116/210	55.4	131/509
Claus	11.6	115/144	50.9	121/551
Gubler	34.6	115/292	59.3	119/596
Morris	19.6	115/174	51.3	117/441
Christen	19.7	115/164	40.5	120/275

7 Kojima's Field Experiments on the Densification of Natural Snow Layers, 1974

Simple field experiments were performed by Kojima (1974) [14] in order to determine the densification strain-rates of natural snow layers under load. Kojima wanted to demonstrate with his experiments that snow load, and not the metamorphism of snow crystals and grains, is the driving mechanism behind layer densification.

Kojima measured the settlement of several layers of a natural snowpack. The layer densities in Kojima's studies varied between 100 and 300 [kgm^{-3}]. He added and subtracted snow at different locations in order to vary the overburden stress. Subsequently, the layers densified at different rates. By analyzing the initial and final layer densities, it was then possible to determine an average settlement strain-rate as a function of the stress. This information was used to formulate a viscosity law for low density snow,

$$\eta = 8.64(10^6)e^{0.021\rho} \qquad [\text{Pa s}]. \qquad (48)$$

In this section, the load subtraction tests of Kojima are simulated using this viscosity law. The notation used by Kojima to designate the tests and layer positions, as well as the initial densities will be taken directly from the original paper.

In the load subtraction experiments a 5 x 1.5 m wide and 1 m deep trench was dug in a level snowpack near Sapporo. On one side of the trench four points were selected where 70 x 70 cm hollows were made by removing snow in the upper part of the snowpack. Each hollow had a different depth. Thus, the snow beneath each hallow was subjected to a different overburden stress. The subtracted loads at the hollows (denoted S-1 to S-4) was 0.16 kPa, 0.33 kPa, 0.67 kPa and 1.07kPa. The points, S-a, S-b, etc., refer to the positions were densification measurements were made.

Kojima provides numerical values of initial and final snow density, time interval (six days for the load subtraction tests), average strain rate, load and settlement at the locations S-b, S-c and S-d. Temperatures were not measured. A comparison between the measured and calculated final layer densities and the total settlement is presented in Table 4.

Table 4. Measured and simulated layer densities and settlements.

Snow Layer	Hallow	Initial Snow Density [kgm^{-3}]	Measured Final Density [kgm^{-3}]	Sim. Final Density [kgm^{-3}]	Measured Settlement [cm]	Sim. Settlement [cm]
S-b	N	138	218	350	13.3	18.0
	S-1	138	197	250	10.7	14.0
	S-2	138	169	195	9.8	11.5
S-c	N	184	250	310	7.5	10.1
	S-1	184	236	265	6.2	7.7
	S-2	184	222	250	6.1	7.4
S-d	N	237	286	310	5.8	7.0
	S-1	237	280	305	5.1	5.2
	S-2	237	282	282	5.0	5.1
	S-3	237	257	257	3.1	3.0

The simulation results for snow layer S-d, located near the bottom of the snowpack, show a very good agreement with the measurements (both densities and settlements). This layer has the highest initial density. The deviation

of the simulation results from the measurements worsens with decreasing initial density. The poorest agreement is at position S-b which is located only 20 cm below the snowpack surface.

In Table 5 a comparison is made between the measured and calculated average strain rates.

Table 5. Measured and simulated average strain rates.

Snow Layer	Hallow	Measured Average Strain Rate $10^{-7}(\mathrm{s}^{-1})$	Simulated Average Strain Rate $10^{-7}(\mathrm{s}^{-1})$
S-b	N	8.87	7.19
	S-1	6.88	6.65
	S-2	3.91	4.16
S-c	N	5.93	6.04
	S-1	4.81	5.39
	S-2	3.65	4.36
S-d	N	3.65	3.68
	S-1	3.20	3.21
	S-2	2.80	2.75
	S-3	1.22	1.14

8   Conclusions

In this paper we have presented a computational procedure to model instationary creep movements in alpine snowpacks. The model allows the treatment of large deformations, strains and strain rates. These processes have never been modelled - or experimentally verified - in any existing 2-D finite element model.

At the present time we are employing a simple Maxwell model to describe the viscous behaviour of snow. This model can only describe snow creep under constant loading. Altough we have shown that the model can simulate the experimental tests of DeQuervain and Kojima, more complicated models must clearly be formulated. For example, the model does not describe snow relaxation under decreasing loading. Therefore, it could never be used to

study the formulation of wet snow avalanches during periods of snow melt. Presently, the model also does not take into account snow microstructure.

Because the procedure is based on the concept of micro-planes, it can be used to model snow fracture and avalanche formation. However, fracture laws are presently failing.

The model employs Green strains and Piola-Kirchhoff stress measures to describe material behaviour. Other stress and strain measures are possible. For example, logarithmic or natural strain measures could be employed in the n-directions. The choice of strain and stress measures will certainly have an influence on the calulated material parameters.

In our validation studies we have found that different viscosity laws are only valid for a particular density and strain rate range. Considerable care must therefore be applied when using the viscosity formulations presented in this article.

We have performed many computational tests with varying number of directions, N. We have found that at around $N = 10$, there is no significant change in simulation results. However, this conclusion might change as more complicated material laws are implemented. For example, when highly non-linear material laws with differing response in tension and compression or material fracture are introduced, the number of material directions N might increase in order to model avalanche formation.

References

1. Lehning, M., Bartelt, P. and Brown, R. (1998). Operational Use of a Snowpack Model for the Avalanche Warning Service in Switzerland: Model Development and First Experiences, *Proceedings of the NGI Anniversary Conference, Norwegian Geotechnical Institute*, May 1998, 169–174
2. Russi, T., Ammann, W., Brabec, B., Lehning, M. and Meister, R. (1998). Avalanche Warning 2000, *Proc. of the int. snow science workshop (ISSW 1998)*, Sunriver, Oregon
3. Smith, F. and Sommerfeld, R. (1971). Finite-Element Stress Analysis of Avalanche Snowpacks, Short Note, *Journal of Glaciology*, Vol. **10**, No. 60, 401–405
4. Curtis, J. and Smith, F. (1974). Material Property and Boundary Condition Effects in Avalanche Snow-Packs, *Journal of Glaciology*, Vol. **13**, No. 67, 99–108
5. Lang, T. and Sommerfeld, R. (1977). The Modeling and Measurement of the Deformation of a Sloping Snow-Pack, *Journal of Glaciology*, Vol. **19**, No. 81, 153–163
6. Bader, H.P., Gubler, H.U. and Salm, B. (1989). Distributions of stresses and strain-rates in snowpacks, *Proceedings of the Conference: Numerical Methods in Geomechanics, edited by Swoboda*, (Innsbruck 1988)
7. de Quervain, M. (1945). Die Setzung der Schneedecke, *Interner Bericht Nr. 11, Eidgenössisches Institut für Schnee- und Lawinenforschung, Davos*, September 1945

8. Salm, B. (1975). A constitutive equation for creeping snow, *IAHS-AISH Publication No. 114, Snow Mechanics Symposium, held at Grindelwald, Switzerland*, April 1974, 222–235

9. Desrues, J., Darve, F., Flavigny, E., Navarre, J. and Taillefer, A. (1980). An Incremental Formulation of Constitutive Equations for Deposited Snow, *Journal of Glaciology*, Vol. **25**, No. 92, 289–307

10. Brown, R. (1977). A Fracture Criterion for Snow, *Journal of Glaciology*, Vol. **19**, No. 81, 111–121

11. Bazant, Z. and Oh, B. (1985). Microplane Model for Progressive Fracture of Concrete and Rock, *ASCE Journal of Engineering Mechanics*, Vol. **111**, No. 4, April 1985, 559–582

12. Bazant, Z. and Prat, P. (1988). Microplane Model for Brittle-Plastic Material: I. Theory, *ASCE Journal of Engineering Mechanics*, Vol. **114**, No. 10, October 1988, 1673–1688

13. Bazant, Z. and Prat, P. (1988). Microplane Model for Brittle-Plastic Material: II. Verification, *ASCE Journal of Engineering Mechanics*, Vol. **114**, No. 10, October 1988, 1689–1702

14. Kojima, K. (1974). A field experiment on the rate of densification of natural snow layers under low stress, *IAHS-AISH Publication No. 114, Snow Mechanics Symposium, held at Grindelwald, Switzerland*, April 1974, 298–308

15. Mellor, M. (1975). A review of basic snow mechanics, *IAHS-AISH Publication No. 114, Snow Mechanics Symposium, held at Grindelwald, Switzerland*, April 1974, 251–291

16. Claus, B. (1978). Compactive viscosity of snow from settlement gauge measurements, *Interner Bericht Nr. 565, Eidgenössisches Institut für Schnee- und Lawinenforschung, Davos*, August 1978

17. Gubler, H.U. (1994). Physik von Schnee, *Interne Herausgebung, Eidgenössisches Institut für Schnee- und Lawinenforschung, Davos*

18. Morris, E.M. (1994). Modelling mass and energy exchange over polar snow using the DAISY model, *IAHS Publication* No. **223**, 53–60

19. Loth, B. and Graf, H.F. (1998), Snow Cover Model for Global Climate Simulations, *Journal of Geophysical Research*, Vol. **98**, No. D6, 10,451–10,464

20. Crisfield, M. (1991). Non-linear Finite Element Analysis of Solids and Structures. Volume 1: Essentials, John Wiley and Sons, Inc., 605 Third Avenue, New York, NY 10158-0012, USA.

21. Haefeli, R. (1942). Spannungs- und Platizitätserscheinungen in der Schneedecke. *Mitteilungen aus der Versuchsanstalt für Wasserbau an der Eidg. Technische Hochschule (Zürich)*, Nr. 2.

22. Jansson, M. (1901). Ueber die Wärmeleitfähigkeit des Schnees, *Ofversigt af Kongl. Vetenskaps-Akademiens Forhandlinger*, Vol. **58**, 207–222

23. Devaux, J. (1933). L'économie radio-thermique des champs de neige et des glaciers, *Ann. Chim. Phys.*, Vol. **20**, 5–67

24. Sturm, M., Holmgren, J., Knig, M. and Morris, K. (1997). The thermal conductivity of seasonal snow, *Journal of Glaciology*, Vol. **43**, No. 143, 26–41

25. Bartelt, P., Christen, M. and Wittwer, S. (1999). HAEFELI, a 2D-snowpack-simulation program - documentation and examples, *Interner Bericht (unveröffentlicht), Eidgenössisches Institut für Schnee- und Lawinenforschung, Davos*, Herbst 1999

26. Salm, B. (1977). Snow Forces, *Journal of Glaciology*, Vol. **19**, No. 81, 67–100

27. Salm, B. (1971). On the Rheological Behavior of Snow under High Stresses, *Contributions from the Institute of Low Temperature Science, Series A* No. **23**, *Hokkaido University, Sapporo Japan*, 1–43

28. Salm, B. (1967). An Attempt to Clarify Triaxial Creep Mechanics of Snow, *from Physics of Snow and Ice, Proceedings of the International Conference on Low Temperature Science*, Volume **I**, Part 2, Edited by Hirobumi Oura